

Transcriptome and Redox Proteome Reveal Temporal Scales of Carbon Metabolism Regulation in Model Cyanobacteria Under Light Disturbance

Short title: Physics-informed machine learning of transcriptome combined with redox proteome analysis of *S. elongatus*

Connah G. M. Johnson^{1†}, Zachary Johnson^{2,3†}, Liam S. Mackey^{4†}, Xiaolu Li², Natalie C. Sadler², Tong Zhang², Wei-Jun Qian², Pavlo Bohutskyi^{2,3}, Song Feng^{2*}, Margaret S. Cheung^{2, 5, 6*},

- 1 Physical and Computational Sciences Directorate, Pacific Northwest National Laboratory, Richland, Washington, United States of America
- 2 Biological Sciences Division, Pacific Northwest National Laboratory, Richland, Washington, United States of America
- 3 Washington State University, Pullman, Washington, United States of America
- 4 Rensselaer Polytechnic Institute, Troy, New York, United States of America
- 5 Environmental Molecular Sciences Laboratory, Pacific Northwest National Laboratory, Richland, Washington, United States of America
- 6 University of Washington, Seattle, Washington, United States of America

* Co-corresponding authors

Email: song.feng@pnnl.gov, margaret.cheung@pnnl.gov

†These authors contributed equally to this work.

Abstract

Central carbon metabolism in model cyanobacteria involves multiple pathways to adapt to energy-light limitations across diel cycles. However, the success in mechanistic modeling for phenotypic prediction of the protein regulators in the metabolic state depends on capturing the vast possibilities emerging from multiple regulatory pathways in complex biological processes. Here, we develop a state-of-the-art approach based on an energy-landscape concept to differentiate interactions involving redox activities as well as conformational changes of proteins and nucleic acids interactions in multi-layered protein-DNA regulatory networks under light disturbance. Our approach is a data-driven modeling workflow using a physics-informed machine learning algorithm to train a non-linear mathematical model for interpreting gene expression dynamics and to lead discovery for protein regulators using redox proteome analysis. We distinguish light-responsive elements within central carbon metabolism pathways from independent variables like circadian time using the publicly available transcriptome datasets of *Synechococcus elongatus* [1] over diel cycles responding to light perturbations. Our approach provides interpretable *de novo* models for elucidating events of reactions in complex regulatory pathways in response to stressful disturbance from the environment. We discovered protein regulators in response to light disturbance in the proteome analysis involving shifts in protein abundance as well as cysteine redox states in *S. elongatus* under constant illumination and after two hours of darkness. We discovered significant shifts in cysteine redox states in regulatory proteins such as transcription sigma factors and metabolic enzymes in the oxidative pentose phosphate pathway and the Calvin-Benson cycle, while the changes in their protein abundance were minimal. These results indicate that regulatory dynamics in reductant generation link photo-induced electron transport pathways and redox metabolic pathways with circadian rhythms through fast redox-induced conformational changes or slow expression regulations across networks, offering a mechanistic understanding of how molecular changes relate to specific phenotypic traits under the light or energy limitations over the diel cycle.

Keywords: physics-informed machine learning, perturbative biology, post-translational modification, cysteine oxidation, systems modeling

Author summary

We constructed a system-level approach to uncover the relationships between molecular and phenotypic changes under light disturbance. We used the publicly available gene expression data of cyanobacteria to train interpretable machine-learning models that generate testable, de novo networks, for elucidating complex reactions in the dynamic regulatory pathways of central carbon metabolism. This model leads to the discovery of protein regulators analyzed by redox proteome analysis. The assemblage of protein regulators direct multiple pathways in accordance with circadian rhythms, offering insights into cyanobacteria's response to light or energy limitations over the diel cycle.

Introduction

As phototrophic organisms, cyanobacteria harvest energy from light to fix CO₂ into glucose which can then be converted to valuable chemical commodities while eliminating the need for sugar feedstocks [2]. However, the inefficiency of the enzymes in the CO₂ fixation pathway limits their utility as a host for biological chemical production [3]. Such a shortcoming motivates the strategies for profiling alternative pathways or using synthetic biology tools to rewire metabolic processes involved in photosynthesis, CO₂ fixation, and carbon metabolism [4]. To address this need, we used the cyanobacteria *Synechococcus elongatus* PCC 7942 (*S. elongatus*) as a tractable model for developing a data-driven modeling with a perturbation biology approach to gain insight about the metabolic processes from multi-omics data.

The advent of multi-omic technologies has ushered in the generation of vast and diverse biomolecular data for profiling biological systems [5]. These multi-omics datasets were often produced within isolated contexts [6], which complicates their integration for mechanistic insights. Moreover, a common approach to modeling metabolic processes at the subcellular level [7-9] involves characterizing the transcriptomic changes induced by systematic treatments or environmental perturbations [10]. These orchestrated response of a cell to stimuli is often regulated by a limited number of transcriptional factors (TFs) that modulate transcription [11-13] through conformational changes in proteins and nucleic acids. Some of these TFs are proteins or enzymes susceptible to post-translational modifications (PTMs) [14], including environmental redox responses via reactive cysteine residue [15]. These PTMs on proteomes further complicate the prediction performance of systems modeling [16].

Such complex processes necessitate the development of nonequilibrium physics frameworks and data-driven machine-learning approaches to dissect the underlying mechanisms of emergent phenomena across scales [17]. On a general framework for discussing reaction dynamics in complex systems [22], new phenomena can rise from the mesoscopic dynamics of intrabasin or interbasin motion on a non-equilibrium energy landscape (**Figure 1A**). There are fast, microscopic dynamics representing reversible redox reactions [19] happening at mixing at a small scale; intrabasin motions within protein conformations [20] at an intermediate scale; and the slow interbasin switching with the kinetic rates exponentially dependent on the system size at a larger scale for biochemical regulations. As noted by Anderson's principle of "More is Different", large-scale behavior emerging from microscopic scales can significantly differ from the small-scale behavior itself [21]. We use light disturbance as a perturbation approach to

differentiate the impact of redox interactions on the protein conformations from the protein-DNA regulatory interactions in multi-layered regulatory networks in **Figure 1B**.

In this work, we aimed to develop a physics-informed machine learning (PIML) [32] approach to learn from the response of TF proteins in changing environments for predicting multiple phenotypes or profiling alternative pathways in regulatory functions. This is achieved by first applying dimension reduction techniques on the large datasets to mitigate computational demand with machine-learning method that incorporates a physical perspective [27], while recapitulating the selected phenotypes responsive to light stimuli as perturbation. To explore a broad parameter space covering a dynamical system of *S. elongatus* periodically facing energy limitation, we analyzed the transcriptome expression profiles under varying light intensities over the circadian rhythms in diel cycles from the public National Center for Biotechnology Information (NCBI) database. The PIML approach (**Figure 1B**) constructs dynamic models with optimal gene interaction parameters in response to light disturbance without relying on *a priori* information about their interaction network. This workflow also takes the redox and global proteome analysis on *S. elongatus* culture after light disturbance to screen for the protein regulars. The redox proteome analysis on the *S. elongatus* culture revealed that the cysteines from four protein regulators showed significant shifts in the oxidation changes, while the relative protein abundance remained similar. These screened regulator proteins are involved in the circadian cycle, oxidative pentose phosphate pathway, and the Calvin-Benson cycle (**Figure 1B**), forming a “timed shunt” for directing biochemical reactions in multiple pathways at the protein structure level through fast redox PTM to support the metabolism of the cyanobacteria model in day-night cycles. Our work highlighted a multilayered regulatory network of central carbon metabolism built on chemical and molecular interactions, coupled to circadian rhythmicity in cyanobacteria, crucial for evolutionary fitness under the periodic light-energy limitations observed in diel cycles. Our approach to integrate -omics data to screen for regulators is organism-agonistic as long as the datasets were accumulated on the basis of a perturbation biology approach.

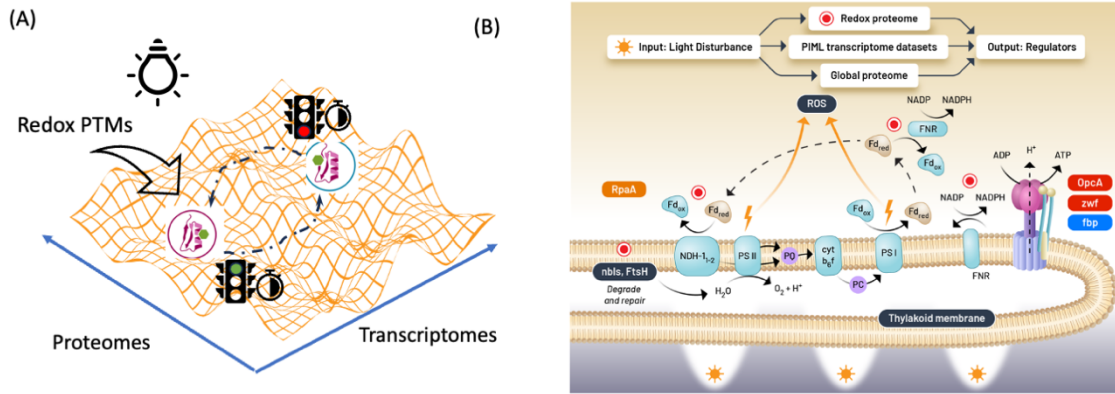


Figure 1. A general framework for reaction dynamics in complex system and paths for an out-of-equilibrium process of electron and energy transport over the diel cycle in *S. elongatus* for carbon fixation. (A) A functional state on the landscape characterized by proteome and transcriptome is represented by the activities of protein structures. Cysteine PTMs on protein structures signal the temporal alternation of the metabolic pathways in phase with the periodic light-energy limitation from the environment. New phenomena, or new metabolic states, can arise from the mesoscopic dynamics of intrabasin or interbasin motion on a non-equilibrium energy landscape under light disturbance. (B) Model cyanobacteria *S. elongatus* serves as a science use case [23-26]. During the day, energy is generated via photosynthesis, with several proteins involved in the transport of electrons and the reduction of electron donors. The photosynthetic electron transport chain begins with photosystem II (PSII) on thylakoids. Cyclic electron flow is another mechanism of electron-energy transport where the cyanobacteria handle stress from light exposure by redirecting electrons from PSI to NDH-1 through ferredoxin (Fd) and plastoquinone (PQ) and splitting H_2O . In our study, we discovered four protein regulators as outputs from the workflow, shown in colored boxes, that collectively responds to cysteine post-translational modifications within two hours of light disturbance from the *S. elongatus* culture, while their relative protein abundance remains similar. The orange box represents RpaA, a master regulator from the circadian cycle. The red boxes represent OpcA and zwf from the oxidative pentose phosphate pathways. The blue box represents fbp from the Calvin-Benson cycle.

Results

Development of an iterative workflow to curate metadata sets by learning dependent variables in the expression profiles responsive to stimuli over diel cycle

We established an iterative workflow of data analysis that utilizes a physics-informed machine-learning (PIML) package, CellBox {Yuan, 2021 #3544}, to curate a set of transcriptome expression data that recapitulates the selected phenotypes responsive to light stimuli as perturbation in **Figure 2**. This package relies on quantitative datasets that observe molecular changes to construct the mathematical representations of dynamical equations for systems modeling and does not require *a priori* knowledge of known molecular interactions to construct a machine-learning model. We used the expression profiles from transcriptomes of the *Synechococcus elongatus* PCC 7942 cyanobacteria [23-26] as phenotypic observables in response to light stimuli in the PIML modeling with CellBox.

The first step of the workflow is to curate a dataset of metadata filtered from the full transcriptome database of *S. elongatus* by a quality control (QC) pipeline for the phenotypic observables in response to light in a dynamic system periodically facing energy-light limitations (see **Section 1** in **S1 Text** for a description of the QC pipeline that filters circadian system experiments from the literature). We transformed the expression profiles of transcriptome dynamics, quantitative observables, and dependent variables over a diel cycle to independent variables (see Section 3 in S1 Text). We used the genes known from the literature to be light-regulated [36] to train the mathematical representation of the governing dynamical equations in the machine learning models (see **Table S1** and **S4**. Homology match between transcription domains and its regulated gene responsible for circadian rhythm adjustments in cyanobacterium *S. elongatus* PCC 7942). This dataset is not directly applicable to training due to weak phenotypic responses to stimuli.

To address this issue, we grouped the phenotypic observables from the curated transcriptomic expressions of *S. elongatus* through two levels of data granularity. The first one, “Gene”, is a fine-grained model of transcriptomic expressions. The other one, “Module”, is a coarse-grained model from which it was created from an independent component analysis (ICA) [34] of the same curated datasets. The Module model is composed of clustered groups, or independent modules (imodules), of transcriptomic expressions, according to the patterns of their expression levels using iModulonDB [10]. Both models were then used as inputs to separately train the mathematical representations of dynamical response by light stimuli using

PIML. We iterated this process and evaluated the learning performance with the Pearson's correlation until the criteria of training were met.

We iterated the step of metadata curation step by updating the filters for sample QC. We used the interpretable outcome as feedback to adjust the sample QC of metadata curation enabling us to gain insight into the contributions of significant elements and interactions between nodes in the resultant network. This updated set of curated datasets was again used as inputs for training with PIML in a Gene or Module model. Iteration stopped when the analysis of the predicted responses returned a validation loss that is less than 100 from the CellBox package. The validation loss in the machine-learning procedure was defined as the Euclidean distance between the physics-informed response model (**Equation 1 in Materials and Methods**) and the experimental reference data.

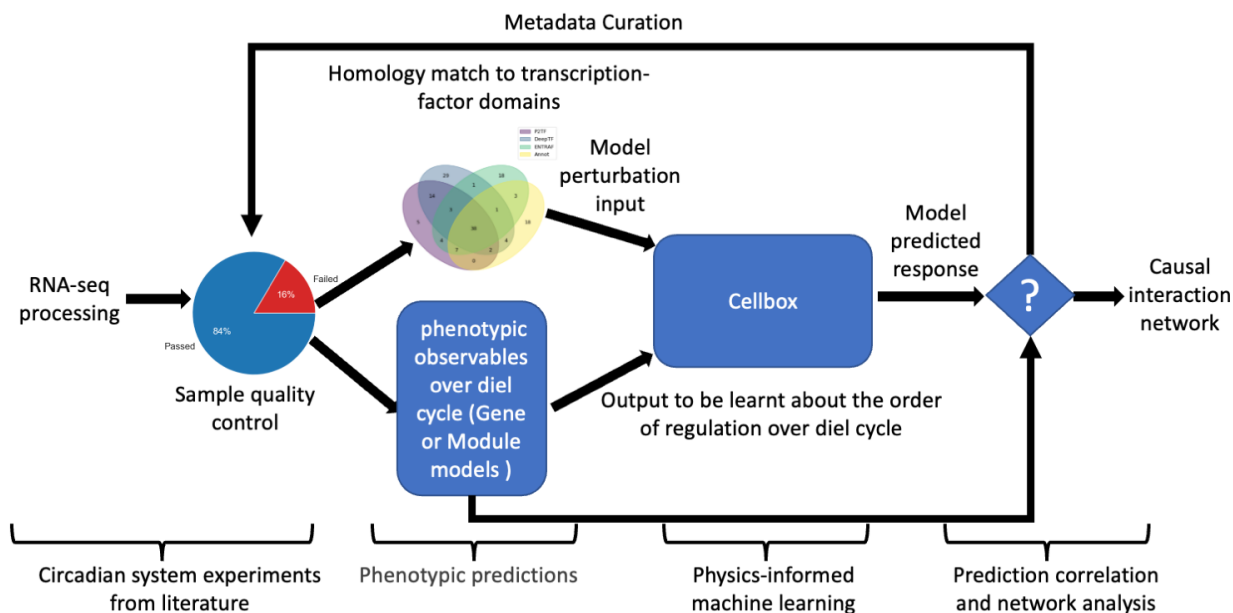


Figure 2. Our iterative workflow for creating a transcriptomic dataset of metadata related to *S. elongatus*. The overall workflow involves iterative steps to create a curated dataset of metadata from the transcriptome in response to light stimuli. We used the gene expression as a proxy for phenotypic observables, grouped in Gene or Module models, over the diel cycle to construct a mathematical representation of dynamical equations using a physics-informed machine-learning (PIML) approach.

The PIML procedure successfully trains the mathematical representations from quantitative datasets for node interactions in response to light disturbance

We showed that the trained models have successfully learned from the quantitative sets in the procedure from Cellbox. The best models from the 1000 simulations from CellBox were compiled to calculate the t-value via a one-sided t-test where the goal was to define interactions that were significantly different than 0. To define significant node interactions, a one-sided t-test was used to query significance in the learnt interaction strengths when compared to the null hypothesis of no interaction. We evaluated the training procedure from CellBox based on the curated data sets with the model learning statistics in **Table 1**. When compared to the phenotypic responses to light in the data (**Figure S1**), both Gene and Module models provided high Pearson correlation statistics of 0.82, demonstrating a successful training of the data-set perturbations from the procedure.

As shown in **Table 1**, the best validation loss (i.e. lowest loss during training) candidate for each parent model was found to be 17.0 for the Module model, with a best testing loss (i.e. loss after testing on fully unseen data) of 412.4 and the best validation loss was 7.6 for the Gene model, with a testing loss of 52.6. These low loss values during the response model training suggests that the parameters were learnt accurately to the reference data. The average correlations between nodes, however, is less significant (~ 0.04),

The Gene model exhibited a testing loss that was 10 times less than that of the Module model when comparing the learnt and training expression values. However, the former had a lower number of 866 successful candidates whose validation loss met an initial cut-off threshold of 1000. This suggests that the larger data dimension of the Gene model required a greater number of network nodes to train and was more difficult to train. The larger data dimension provided more flexibility in the parameter search landscape at the cost of an increased computation time signified by fewer successful candidates. Although the Module model provided a greater number of 4762 successful candidates it resulted in larger validation and testing losses. In summary, the Gene model returned fewer candidates due to increased model complexity that grows with the number of nodes training on a large dataset of genes. The candidates for the smaller dataset in the Module model based on the groups of genes that share regulatory functions were more readily trainable, indicating that the Module and Gene models differed in the accuracy and training time.

The training procedure is described in the **Materials and Methods** section.

Model	Module	Gene
Number of candidates	4762	866
Best validation loss	17.00	7.60
Best testing loss	201.71	26.43
Pearson correlation	0.82	0.82

Table 1: Summary of the statistics of the mathematical models trained by CellBox using the best curated datasets from the transcriptome. The mathematical models were trained on a fine-grained “Gene” model as well as a coarse-grained “Module” model of the best curated datasets of metadata.

The master regulator of circadian control, RpaA, is among top ranked imodules from the curated metadata sets

We evaluated the modular gene constituents from the curated metadata of successful training procedures using ICA. ICA groups regulatory genes into independent modules, providing a “coarse-grained” view of the complex data structure in the curated datasets.

Gene set enrichment was computed at a false discovery rate (FDR) of 1×10^{-3} for functional gene sets, considering a maximum of two regulators for a given imodule for transcriptional regulatory network (TRN) enrichment and taking the lowest scoring q-value as the regulator set. The procedure to include gene into the module and the enrichment of transcription factors (TFs) with functional activity are described further in **Section 2** in **S1 Text**. Collectively, the independently regulated modules decomposed by ICA accounts for 71.82% of the variance in the gene expression dataset. A total of 63 imodules were defined with an average module size of 18 genes in each module (**Figure 3A**).

The top ten imodules, or referred as “phenotypes”, account for the largest proportion of the variance in the curated dataset. They were further characterized according to their associated gene sets with TF regulators and functional metabolic roles by enrichment analysis (**Figure 3B**). Imodules 50 and 62 cumulatively explain 14.2% of the gene expression variance. These imodules were enriched in the gene targets of the RpaA master regulator of circadian control [36], with 16 and 18 known gene targets associated with imodules 50 and imodule 62, respectively. Each of these imodules was similarly associated with a secondary regulator, SigF2 for imodule 50 and Crp for imodule 62. The targets of SigF2 were also significantly enriched in imodule 6. The imodule that explained the second greatest proportion of variance,

imodule 38, was associated with the gene targets of both RpaA and RpaB, while imodule 45 was enriched for the gene targets of RpaB in association with PedR. The remaining imodules associated with known regulators, imodules 24 and 52, were enriched in gene targets from Rre1 and NtcA, respectively.

Imodules that were not enriched for known regulators were characterized based on functional enrichments. Imodule 1 was significantly enriched with genes associated with oxidative phosphorylation, while imodule 27 was enriched in genes associated with photosynthesis. Imodule 56, labeled “Unknown”, was the only imodule that was not associated with a known regulator or functional pathway.

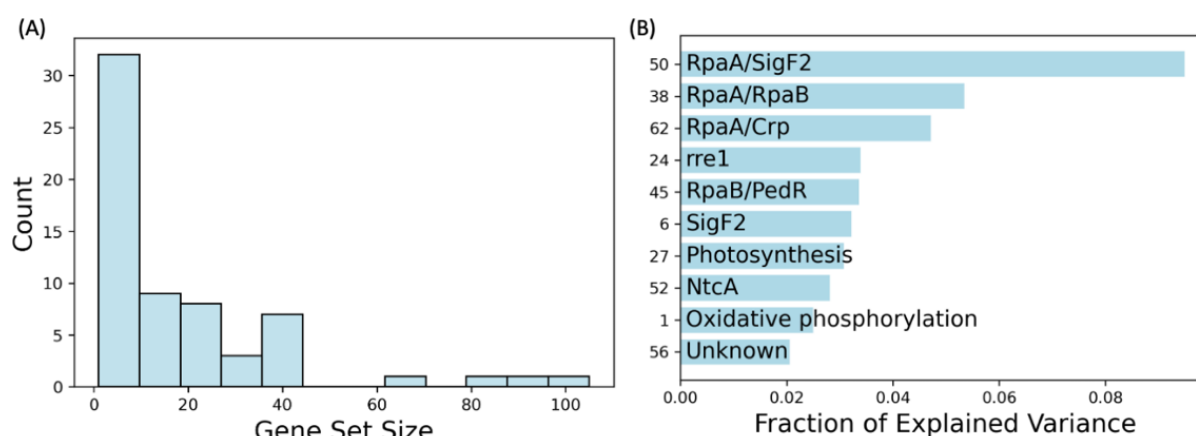


Figure 3. Grouping of imodules from the curated metadata. Curated transcriptomic datasets of metadata were reduced to a modular dataset of annotated transcription factors under the light perturbation. (A) The distribution of the imodules according to the size of the gene members. (B) The top 10 phenotype imodules capture key regulatory processes.

The interpretable PIML de novo network models capture directed connections to known regulators stimulated by light

A set of ordinary differential equations with a nonlinear envelope was used to simulate the dynamic response with CellBox as a PIML tool that learned the parameters of interaction strengths between entities in a de novo network model. Because of the interpretable outcomes from PIML, a great extent of regulatory dynamics connecting to prior knowledge about the pathways responding to light stimuli from an informative set of curated transcriptome expressions over the diel cycle was revealed by comparing the nodes with a set of known regulatory genes from the literature (i.e. regulons, **S1 Table**).

We illustrated *de novo* multilayered networks in **Figure 4** from the best training models in **Table 1**. The nodes numerically labeled are imodules, and the ones alphabetically labeled are genes in a network. The edges between nodes show directed interactions learned from training in response to light perturbation. The nodes and edges in blue colors signify known regulons (see **S1 Text** and **Table S1**). We colored the nodes and edges orange for those that are potentially new connections to other regulatory pathways coupled to light perturbation. The networking architecture allows the propagation of the response over the components of imodules (i.e. a group of genes) in the Module model (**Figure 4A**). Comparatively, it propagates through genes in the Gene model in **Figure 4B**. The former provides a “coarse-grained” view of the interactions for interpretation, while the latter is rather “fine-grained”. Below, we showed that both models can capture the literature-provided interactions. In the Module model, there are 102 observed nodes, of which 40 were gene expression and 59 were module response. In the Gene model, there are 872 observed nodes, of which 40 were TF expression and 829 were gene expression. We have selected the top-ranked nodes, in terms of significant expression, in the *de novo* networks for further analysis of relational interactions.

In **Figure 4A**, most imodules are of known experimental importance, or “regulons”, colored in blue. Indeed, imodules 50, 38, and 6 indeed are accounted for among the top explained variances from the ICA analysis (**Figure 3**), while some other nodes in the network are individual genes. These connected nodes in a directed graph reveal a simplified regulatory network with key members. We traced the blue edges from the phenotypic imodule 50 (enriched by RpaA and SigF2), it connects with the two known circadian regulators genes, RpaA (labeled “b”) and SigF2/SigJ (labeled “h”) (**Figure 3B**). Through the “b” node of RpaA, imodule 50 connects to another imodule 38 which is comprised of RpaA and RpaB. This directed graph of the *de novo* network captures the known relational interaction between the sigma factor regulation and gene expression of RpaA for the circadian rhythm in *S. elongatus* through an interwoven web of direct and indirect relationships [26]. The mathematical models capture the perturbation effects from light stimuli, even though these imodules are not in direct relation to the light source.

The Gene model (**Figure 4B**) reveals a greater number of nodes than that for the Module model (**Figure 4A**), as the former represents the nodes at a more granular detail about the direct interactions than the latter. Among the known genes in the interaction networks that are responsive to light stimuli in **Figure 4B**, the RpoD5 sigma factor (labeled “d”) connects to two other conserved hypothetical proteins (labeled

“u”) and Smc (labeled “x”). However, the fine-grained view lacks the representation of higher-order connections through the propagation of direct interactions because the interactions between entities are comparably weak. This is manifested by the histogram of the Pearson correlation coefficients between the predicted and observed expressions for each node in the *de novo* networks in **Figure 4 (C)** and **(D)** for the Module and Gene models, respectively. Although the correlation coefficients are higher for the nodes from both *de novo* networks than those representing the known TFs alone (TF, in green), the distribution of correlation coefficients is broader for individual genes (**Figure 4D**) than that for imodules in **Figure 4C**, inferring a weaker parameter interaction for the former. As a reference, a nodal correlation coefficient of 1 is shown for the perturbation nodes (in purple).

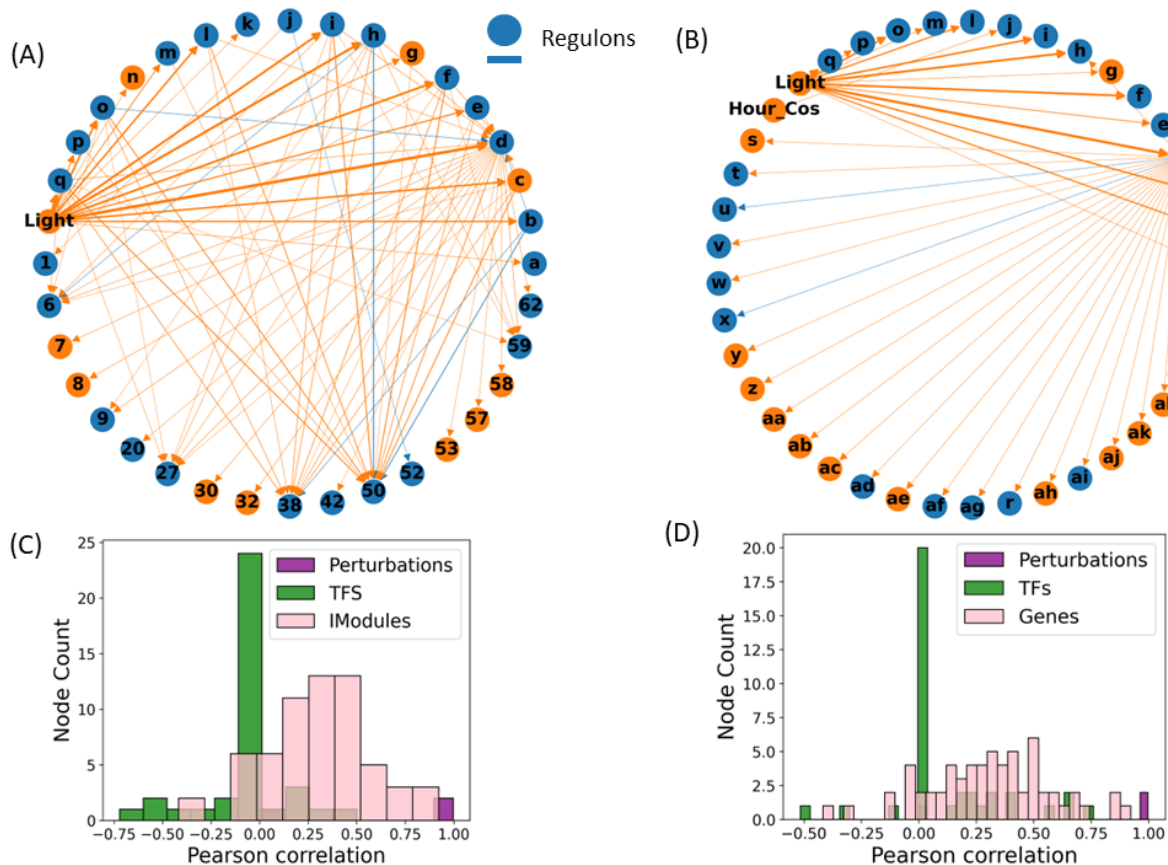


Figure 4. Comparison of gene interactions for the Module and Gene models. The interactions between entities in the (A) Module model and (B) in the Gene models are revealed by a directed graph from a simplified regulator network responsive to light stimuli. (C, D) Histograms of the node counts sorted by the Pearson correlation coefficients between the predicted and observed expression levels for each node for transcription factors (TFs) or perturbations.

The interpretable PIML *de novo* network infers interactions that connect known regulators stimulated by light to multiple pathways including central carbon metabolism

The *de novo* networks inferred from informative transcriptome datasets with PIML models reveal far more relational interactions (for nodes or arrows colored in orange in **Figure 4**) than known direct or indirect interactions responsive to light stimuli over the circadian time. The constructed *de novo* networks of dynamic models discover new connections (shown by orange nodes and edges) from known regulators (shown by blue nodes and edges), inferring that the propagated gene expressions are responsive to light perturbation. A “zoomed out” coarse-grained view of the network in the Module model in **Figure 4A** shows that the responsive nodes are involved in the circadian regulation as well as metabolic pathways. A group of TFs from imodule 50 are connected to response regulator *srrB* (labeled “q”), a putative transcriptional regulator TetR (labeled “i”) and glucose 1-dehydrogenase *dgh2* (labeled “c”). Those of imodule 38 are also connected to *srrB* (labeled “q”) alongside the sigma factor RpoD6/SigA6 (label “o”), and the circadian clock protein kinase KaiC (labeled “f”). Additionally, imodule 6 is connected to RpoD6/SigA6 (labeled “o”), *dgh2* (labeled “c”), and another sigma factor RpoD5/SigC (label “d”). Interestingly, all three major imodules 50, 38, and 6 are connected to TetR (labeled “i”). While TetR is not directly responsive to other genes under light perturbation in **Figure 4B**, the interpretation from the analysis signifies multilayered networks where TetR possibly plays a pivotal role in regulating multiple pathways.

In the fine-grained Gene model, this *de novo* network also inferred a large set of previously unknown relational interactions between the “d” node (representing RpoD5) and other genes manifested by the orange nodes and edges. Among these inferred interactions with the “d” node, they connect to multiple pathways across subcellular locations (**Table 3**) including cytosol (e.g. *zwf*, labeled “ak”, from the glycolysis), membranes (e.g. cytochrome c oxidate subunit II, labeled “ao” from the membrane), or thylakoid membranes (e.g. ferredoxin-plastoquinone oxidoreductase subunit D1, labeled “af”, from the cellular thylakoid membrane). Interestingly, the *de novo* model also inferred connections from gene regulation through the “d” node of RpoD5 to several down-regulated pathways in central carbon metabolisms, including the glycolysis through the “ak” node of *zwf*, *OpcA* (labeled “ai”), the oxidative pentose phosphate pathway (OxPPP) through the “ai” node of *OpcA*, and the Calvin cycle through the “aj” node of *fbp*. the interpretation of the connected nodes in the *de novo* network also inferred a relation between the circadian time (“Hour_Cos”) and the global nitrogen regulator *ntcA* (labeled “j”).

Some of these interactions connect TFs that regulate gene expressions to down-regulated enzymes or protein regulators in several in central carbon metabolisms. Because we were interested in understanding the correlation between light responses (mediated by RpaA, OpcA, zwf and fbp) and multiple pathways in central carbon metabolism, we created an illustration of the overlapping pathways that involve these entities in **Figure S2** in **S1 Text** consisting of the Calvin-Benson cycle, glycolysis/gluconeogenesis, OxPPP, sucrose biosynthesis, and glycogen synthesis/degradation. Although their biochemical reactions are not directly initiated by light, their regulations that happen in cytosol may be promptly impacted by reactive oxygen species (ROS), products of photosynthetic reactions, that give rise to multiple phenotypes represented by cellular redox homeostasis in photosynthetic organisms [37]. This information connecting light stimuli to metabolic genes over circadian time allows us to test a hypothesis that redox post-translational modifications (PTM) influence the activities of proteins that regulate overlapping pathways from the central carbon metabolism over the diel cycle.

Node label	Gene ID	Gene name	Description
a	Synpcc7942_0677	pex	Circadian period extender
b	Synpcc7942_0095	RpaA	Two component transcriptional regulator, winged helix family (TR) circadian rhythm response regulator, cytoplasm
c	Synpcc7942_1573	dgh2	Glucose 1-dehydrogenase NAD(P)-dependent
d	Synpcc7942_1849	RpoD5/SigC	Group 2 polymerase sigma factor sigA5
e	Synpcc7942_1108	Hbs1	Histone-like DNA-binding protein, cytosol
f	Synpcc7942_1216	KaiC	Circadian clock protein kinase
g	Synpcc7942_0110	XRE	Transcriptional regulator, XRE family
h	Synpcc7942_1784	SigF2/SigJ	Group 3 RNA polymerase sigma factor SigF
i	Synpcc7942_0599	TetR	Putative transcriptional regulator, TetR family
j	Synpcc7942_0127	ntcA	Global nitrogen regulator, cytosol
k	Synpcc7942_1453	RpaB	Global nitrogen regulator, protein-DNA complex, cytosol
l	Synpcc7942_0703	DprA	DNA processing protein, putative
m	Synpcc7942_0569	RpoD4/SigA4	Group 2 RNA polymerase sigma factor, cytoplasm
n	Synpcc7942_1923	SigG	Group 3 RNA polymerase ECF-type sigma factor
o	Synpcc7942_1557	RpoD6/SigA6	RNA polymerase sigma factor group 2 RNA polymerase sigma factor
p	Synpcc7942_2248	Hbs2	Histone-like DNA-binding protein, cytosol
q	Synpcc7942_0556	srrB	Response regulator, protein-DNA complex, cytosol

Table 2. Descriptions of the node labels in **Figure 4A**. The node labels refer to the gene names from *S. elongatus*. A named protein and its subcellular location may be also provided in the description.

Node label	Gene ID	Gene name	Description
r	Synpcc7942_2306	DnaJ	Heat shock protein DnaJ-like
s	Synpcc7942_0035	Lip	Conserved hypothetical protein (lipoprotein)
t	Synpcc7942_0304	Coq4	Conserved hypothetical protein (coenzyme Q biosynthesis protein)
u	Synpcc7942_0316	–	Conserved hypothetical protein
v	Synpcc7942_0551	MMPL	Conserved hypothetical protein (MMPL domain-containing protein), membrane
w	Synpcc7942_0700	UspA	Conserved hypothetical protein (universal stress protein)
x	Synpcc7942_1397	Smc	Conserved hypothetical protein (chromosome partition protein Smc)
y	Synpcc7942_1464	SomA (1)	Outer membrane porin protein, membrane
z	Synpcc7942_1610	pntB	Pyridine nucleotide transhydrogenase beta subunit, cell inner membrane
aa	Synpcc7942_1611	pntA-2	Nicotinamide nucleotide transhydrogenase alpha subunit-like, cell inner membrane
ab	Synpcc7942_1612	pntA	Pyridine nucleotide transhydrogenase alpha subunit, plasma membrane
ac	Synpcc7942_1635	SomB(2)	Probable porin, major outer membrane protein
ad	Synpcc7942_1656	katG	Catalase-peroxidase, cytosol
ae	Synpcc7942_1757	PriA	Replication restart DNA helicase
af	Synpcc7942_1976	ndhD1	Ferredoxin-plastoquinone oxidoreductase subunit D1, cellular thylakoid membrane
ag	Synpcc7942_2267	–	Hypothetical protein (chromosome segregation ATPase)
ah	Synpcc7942_2307	HNHc	Conserved hypothetical protein (HNHc domain-containing protein)
ai	Synpcc7942_2326	SIMPL	Conserved hypothetical protein (SIMPL domain-containing protein), membrane
aj	Synpcc7942_2333	OpcA	OxPP cycle protein [38] (G6PD assembly protein)
ak	Synpcc7942_2334	zwf	Glucose metabolism Glucose-6-phosphate 1-dehydrogenase (G6PD), cytosol
al	Synpcc7942_2335	fbp	Calvin cycle Fructose-1,6-bisphosphatase F-II, cytoplasm
am	Synpcc7942_2352	yfiA	Putative sigma 54 modulation protein/ribosomal protein S30EA, cytoplasm
an	Synpcc7942_2388	oxdC	Oxalate decarboxylase, outer membrane-bounded periplasmic space
ao	Synpcc7942_2602	ctaC	Cytochrome c oxidase subunit II, multi-pass membrane

Table 3. Descriptions of the labels in **Figure 4B**. The node labels refer to the gene names from *S. elongatus*. A named protein and its subcellular location may be also provided in the description.

The redox proteomes narrow screening for protein regulators in central carbon metabolic pathways of *S. elongatus* revealed by light disturbance

We next employed proteomic-based approaches aimed at investigating the dynamics of redox modifications after light/dark stimuli and monitored the cellular redox state *in vivo*. We cultured *S. elongatus* under constant light followed by a short-term (i.e. 2-hour) deprivation of light as perturbation. We focused on redox PTMs on cysteines mediated by ROS constitute a major mechanism during photosynthesis [39]. It is fast for redox PTM to respond to ROS changes. It takes much less time to influence the regulation over multiple pathways than needing other enzymes for catalysis.

We profiled the changes in the cysteine oxidation level from the redox proteome and the changes in the protein abundance from the global proteome analysis. We first identified that the proteins with redox PTM expressions changed significantly under the light/dark perturbations and compared them against the *de novo* models from the transcriptome analysis in a word cloud format (**Figure 5A**). The redox changes in RpaA, fbp, zwf, and OpcA are significant, but their changes in the protein abundance are not (cutoff: p-value < 0.05, log2FC > 0.1 or < -0.1) (**Figure 5B**). The oxidation level at multiple Cys sites of these proteins changed significantly by light disturbance, suggesting a rapid signaling mechanism by redox PTM. Intriguingly, the expression of cysteine PTM on the gene product of fbp, a protein regulator in the Calvin-Benson cycle, became more oxidized (red) as the system changed from light to dark. In contrast, the expression of cysteine PTM on the gene product of zwf, a protein regulatory in the oxidative pentose phosphate pathway (OxPPP), became more reduced (blue). The cysteine-rich OpcA showed both an increase and decrease in cysteine PTM expression, indicative of the constitutive role of the *opcA* gene, a “class 2” circadian regulator, in shunting multiple pathways in the central carbon metabolism for biochemical processes in response to circadian rhythmicity under limited light energy.

We also discovered few proteins in which the redox PTM and abundance changed significantly. The function of these proteins is to interact with DNAs directly such as PriA, a DNA helicase. Therefore, we do not take them into account when testing our hypothesis. In summary, the proteomic experiments, and *de novo* models from PIML were used in a novel way to infer the mechanisms that influence multiple pathways from central carbon metabolism in response to light disturbance.

(A)



Word cloud of redox proteome changes over the informative transcriptome expressions responsive to light stimuli over diel cycle

(B)

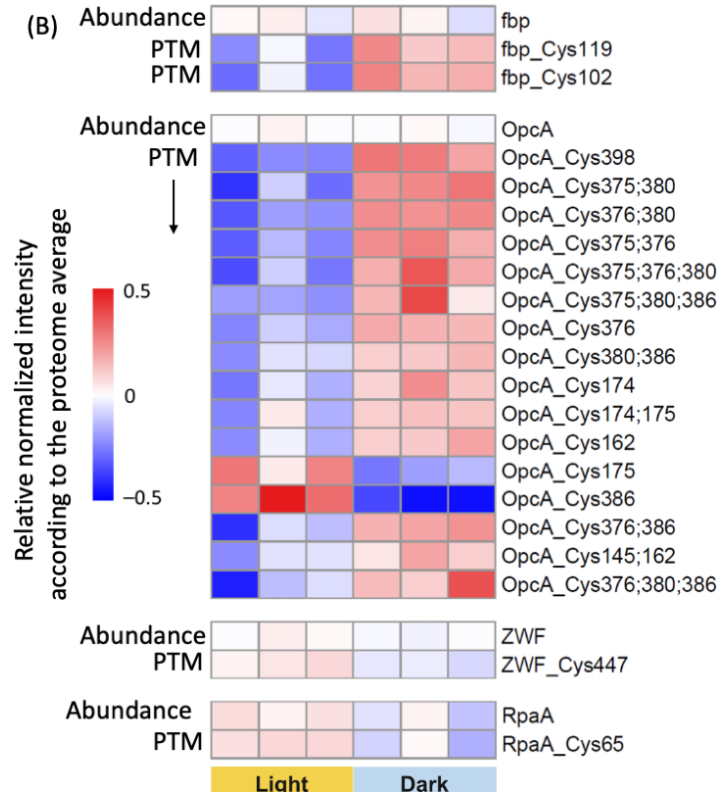


Figure 5. Identified proteins with redox post-translational modification (PTM) expressions that changed significantly under light/dark perturbations. (A) A word cloud was used to gain mechanistic insights into the significance of gene responses under light/dark perturbations. Gene expression responses to light stimuli are derived from the curated dataset of metadata, with those capturing the significant changes in the protein PTMs as revealed by the redox proteomics experiment colored in orange. (B) The heat map of normalized intensity from two kinds of proteome experiments illustrates the variations in the observations. The blue to red scale represents normalized intensities of relative protein abundance (i.e. 1st row of each protein heatmap) and cysteine oxidation level (i.e., cysteine PTM, from the second row to the last of each block). The normalized intensity was scaled by log2. The left three columns of the heatmaps are the replicated measurements under light conditions and the right three columns are measurements under dark conditions taken two hours after switching from constant light exposure.

Discussion

The PIML workflow offers interpretable de novo network models from curated transcriptomic expression datasets

The workflow we developed based on PIML using the CellBox package enabled humans to understand the data through mathematical physics models and lead to the discovery of regulators. PIML[32] offers valuable interpretability compared to autoencoders, although autoencoders are a common deep learning tool. Autoencoders embed the datasets into a latent space representation for mapping features from data structures themselves, acting like a “black box” that lacks explainable features for mapping the output back onto the initial datasets. Constructing explicable machine-learning models that predict complex outputs from correlated datasets remains a critical challenge due to the nonlinear contribution of input feature changes to the output [30, 31]. This complexity creates a growing tension between the accuracy and interpretability of model predictions, especially for a cyanobacteria model with multiple phenotypes, or metabolic states, resulting from the dynamic response of complex regulatory processes.

CellBox was first designed to interpret molecular variations from omics datasets by attributing variations to specific and well-defined phenotypes, such as those used for drug screening in cancer research [29]. Microbial transcriptomic expressions are not direct applications due to: (1) the database encompasses multiple phenotypes, and (2) they often lack information of time-series responses to systematic perturbations. Moreover, it is challenging to establish a mathematical physics model with relational interactions based solely on gene expressions to explain the meaning of observations in a biological process when these sequencing experiments offer sparse transcriptome datasets.

Here, we used three strategies to overcome these deficiencies: (1) We leveraged a full range of transcriptomic datasets of *S. elongatus* cyanobacteria from published databases as a tractable model to develop our workflow. (2) We remedied the sparsity of the transcriptome dataset by using the iModulon [8] to reduce the data dimensions by grouping genes into functional clusters (**Figure 3**). (3) We followed light-dependent reactions such as photosynthesis as dependent variables to set up light stimuli as perturbations to track the propagation of events. Since these reactions are well-documented for studying this cyanobacteria’s circadian cycle that offers time-related information, we aggregated these gene expressions as phenotypic observations over a diel cycle to train the physics model with CellBox.

Our PIML workflow (**Figure 2**), which offers interpretable *de novo* network models, presents a paradigm shifts in terms of the investigative power of regulation analysis. With this workflow, we created two versions of *de novo* regulatory networks, the Module and Gene models, from the same curated dataset. The *de novo* networks are represented as directed graphs with connections between nodes, allowing interpretation of relational interactions from direct or indirect paths. Both Module and Gene models learned from curated datasets provide valuable insight into the interpretable outcomes of PIML, offering a fine- or coarse-grained view of the regulatory network at a hub (e.g. a group of genes such as a regulon) or at a gene scale, respectively, over a network architecture. The Module model revealed a multilayered web of interactions between imodules while the Gene model revealed directed regulations between genes. Both models not only captured known interactions between TFs, but also inferred new connections to others in a *de novo* network. There are tradeoffs, however, in terms of the computational cost as the Gene model that provides a fine-grained view of the data structure increases training difficulty. Nevertheless, all simulations were completed less than a week on high-performance computing clusters.

The *de novo* networks revealed multilayered regulations of central carbon metabolism of *S. elongatus* for the efficient energy utilization in a light-energy-limited environment.

We constructed a data-driven workflow to create simplified *de novo* networks that recapitulate the regulation of carbon fixation and reveal the relational interactions among the genes or imodules under light disturbance. The curated transcriptome datasets encompass regulatory gene networks and several overlapping enzymatic reactions within the central carbon metabolisms. These include light-dependent or -independent redox regulation of photosynthetic electron transport, the Calvin-Benson cycle, and starch biosynthesis (**Figure S2 in S1 Text**).

The Module model provides a global picture of a complex cascade of regulatory interactions, including a circadian rhythm that alternates the daytime and nighttime metabolic mechanisms for survival. Some of the imodules from the same strain of the cyanobacteria {Choe, 2024 #3542} were also recently

identified by the Palsson group using only the ICA approach over the entire transcriptome data. Compared to their study, our datasets were much reduced after PIML training and captured only those that are relational and most responsive to light perturbation. To this end, we embarked on the master circadian regulator RpaA [41, 42]. It regulates a secondary master circadian regulator RpaB [43], which in turn binds with several downstream global regulators such as sigma factors that trigger a complex flow of regulatory actions [44]. In the daytime, the reductants produced from photosynthesis are consequently used for carbon fixation and glycogen synthesis via the Calvin-Benson-Bassham cycle. In darkness, cyanobacteria rely on the oxidative pentose phosphate pathway (OxPPP) [45] to produce reductants in the form of NADPH and downregulate DNA replication [46, 47] to conserve energy [45, 48] and to detoxify ROS when photosynthesis is not active. The coarse-grained de novo network (the Module model in **Figure 4A**) revealed a direct interaction from the light node to the sigma factor, SigF2 and master circadian regular, RpaA. From these direct interactions, we discovered several other indirect interactions through grouped imodules such as 50, 38, and 6. Together, they profiled a hidden puppeteer of TetR (labeled “i”) by sourcing their common regulator from the de novo network. Interestingly, by detecting cellular acetyl-CoA, NAD⁺, and acetyl-phosphate from the metabolic state, the lysine acetylation of the TetR related transcriptional regulator [40] directly adjusts gene expression to changing environmental conditions. The de novo network infers TetR to be a node connecting other metabolic pathways regulated by lysine acetylation to circadian rhythmicity and photo-induced reactions.

In contrast, the fine-grained de novo network presented by the “Gene” model revealed far more hidden interactions between genes than the known ones in **Figure 4B**. The “d” node is a Sigma Factor that downregulates almost every node on the graph with high confidence. We annotated the subcellular locations of the gene products in **Tables 2** and **Table 3**. Interestingly, the downregulated gene products are spread throughout the interior of the model cyanobacteria, including the inner membranes, cytosol, thylakoids, and DNAs. The gene product Smc, labeled “x”, is chromosome partition protein involved in the structural maintenance of chromosomes [49]. The inference from regulating genes to the spatial complexity of morphological phenotypes indicates a dynamic link between gene regulation and cell growth optimized by circadian rhythmicity in cyanobacteria adapting to light-energy limits from environments.

Tracking dynamic redox reactions in response to light disturbance effectively integrates transcriptome and proteome datasets in cyanobacteria and leads to the discovery of protein regulators

We used the curated transcriptome datasets as a guide to develop a hypothesis about the proteins whose chemical activities are in action after light disturbance on a non-equilibrium energy landscape (**Figure 1A**). We hypothesized that the time required to change protein abundance would be longer than the time required for changes in protein redox states under light stimuli, due to the elaborate mechanisms involved in protein synthesis compared to the prompt cellular redox reactions. The former represents slow regulatory responses through protein-DNA binding that involves conformational changes such as protein folding and DNA bending dynamics. In contrast, the latter follows photo-induced electron transfer that suddenly changed a large amount of ROS and protein redox states.

We tested this hypothesis and compared the global and redox proteome for the gene products from the curated transcriptome datasets. After two hours in darkness from constant light exposure, we discovered a few gene products, namely fbp, OpcA, RpaA, and ZWF, with significant changes in the cysteine oxidation level, while there were insignificant changes in their protein abundances, as presented in a word cloud format (**Figure 5A**). This signifies the assemblage of the four protein regulators operate in an immediate time scale involving structural dynamics of proteins with PTMs in biochemical reactions.

We highlighted the potential overlap and distinctions between light-driven regulations at the expression level and redox-dependent regulations at the protein structure level in *S. elongatus*. Fast redox reactions occur through cysteine PTMs that alter structural complexes and dynamics, offering a rapid and specific response to environmental stress from reactive oxygen species (ROS). To this end, tracking the redox reactions in response to light effectively integrate information from transcriptome and promptly screens for regulators in the redox proteome datasets. By combining TF action information with machine learning, our approach provides a novel set of tools to drive insights into complex cell responses and enable new discoveries in gene regulatory interactions.

“Circadian rhythmicity interchange” assemblage connects an inbound photoinduced electron transfer highway and an outbound reduction-oxidation reaction highway to multiple phenotypes in the central carbon metabolism of *S. elongatus*

We speculated that the assemblage comprising of RpaA, fbp, zwf, and opcA play a critical role in directing the upstream electron-energy transfer pathways and the downstream carbon metabolism pathways. Each gene product comes from different pathways and together they form a functional construct similar to an “interchange” on the junction of road transport with busy traffic (**Figure 6**). This surprising discovery suggested, within the first two hours, that these four protein regulators respond to light disturbance through fast cysteine modifications on protein structures, rather than through gene regulations.

This interchange is regulated by cyanobacteria’s circadian timed through RpaA. RpaA (regulator protein of phycobilisome association A) is a master circadian regulator of phycobilisome, a megacomplex on the thylakoid. De novo modeling infers that the regulatory protein of circadian control (RpaA) indirectly coordinates the genes (opcA, fbp and zwf) encoding enzymes in the two alternating pathways for producing reductant NADPH during the day-night cycle. A gene product of fbp is Fructose-1,6-bisphosphatase class 1 [50, 51], known as a redox-sensitive protein in the Calvin-Benson cycle (CBC) whose activity can be regulated by light. A gene product of zwf is glucose-6-phosphate 1-dehydrogenase (G6PD). OpcA[52], an allosteric effector mediating the activity of G6PD, activates the pentose phosphate pathway when light-derived energy is not available [52]. A cysteine-rich regulatory protein, OpcA, is speculated to shunt biochemical reactions in the Calvin-Benson cycle and the oxidative pentose phosphate pathway (OxPPP) through cysteine PTMs.

In our redox proteome study after light disturbance, we revealed the opposing changes in cysteine oxidation activities on cysteines for the gene products of *fbp* and *zwf* (**Figure 5B**), while *OpcA* carried multiple redox shifts in either more reduced or more oxidized tendency. We speculated that *RpaA*, *OpcA*, *ftp*, and *zwf* form a “circadian rhythmicity traffic interchange” to transport electron-energy from inbound photo-induced reaction “highways” to outbound redox reaction “highways” (**Figure 6**). The output of metabolic states is directed by cyanobacteria’s circadian, *RpaA*, that directs reductants from fast electron-energy reactions dependent to the availability of light to the central carbon metabolism via timed alternating pathways – CBC and OxPPP -- with overlapped biochemical reactions. Our work elucidated the assemblage of circadian rhythmicity interchange as a module that interacts with other cellular processes such as photosynthetic light reactions, the electron transfer chain, and cellular metabolism via redox post-translational modification into a broader cellular context [53]. We argued that the energy-landscape concept [17] provides the framework to describe complex reactions built on distinct time scales of chemical and molecular interactions in non-equilibrium cellular processes crucial for cyanobacteria’s entrainment to the periodic light-energy limitations observed in diel cycles [45].

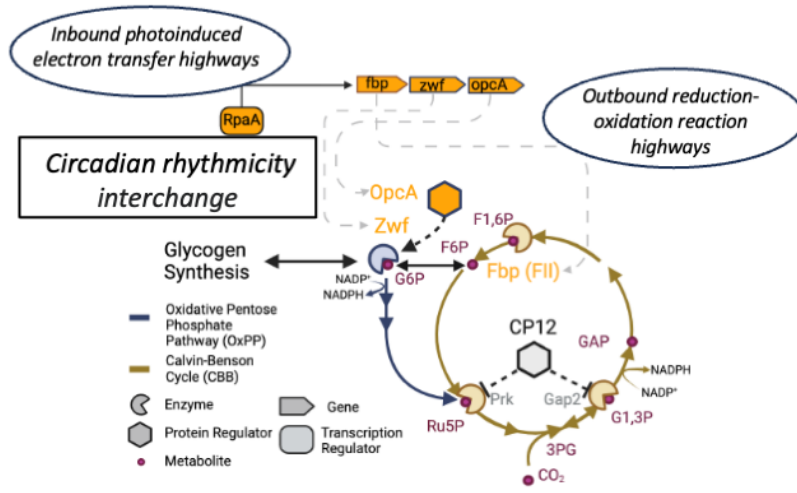


Figure 6. Circadian rhythmicity interchange in *S. elongatus*. A conceptual map of circadian rhythmicity *interchange* connects an inbound photoinduced electron transfer highway and an outbound reduction-oxidation reaction highway to multiple phenotypes in the central carbon metabolism of *S. elongatus*. The assemblage of *interchange* comprises RpaA, fbp, zwf, and opcA (shown in orange). The redox of cysteine PTMs on these gene products, or proteins, signals and coordinates the inbound electron transfer pathways and outbound central carbon metabolism responsive to light disturbance. A cysteine-rich regulatory protein, OpcA, is speculated to biochemical reactions in the Calvin-Benson cycle and the oxidative pentose phosphate pathway (OxPPP) through cysteine PTMs. Our study infers that the regulatory protein of circadian control (RpaA) indirectly coordinates the genes (opcA, fbp and zwf) encoding enzymes in the two alternating pathways for producing reductant NADPH during the day-night cycle.

Conclusion

Understanding how cells respond to environmental stimuli is foundational for guiding the bioengineering of desirable phenotypic behaviors [54, 55]. To this end, we developed a paradigm-shifting framework that combines a deep-learning neural network with a physics-informed mathematical model to quantitatively predict cellular responses to perturbations from large datasets. This approach is aligned with emerging quantitative biology methods that aim to extract dynamical and mechanistic information from 'big data' for cellular processes [56]. Our workflow, enhanced with the PIML models, integrates transcriptome and proteome datasets in cyanobacteria to track dynamic redox reactions in response to light disturbance. We elucidated cellular response to perturbations through a nonlinear kinetic model of genetic expression without prior knowledge of the genes and transcription factor interactions. This flexibility allows the application of our approach to large datasets, enabling the construction of fine-grained or coarse-grained *de novo* regulatory networks with interpretable outcomes.

By analyzing global and redox proteomes from *S. elongatus* culture samples exposed to two hours of darkness after constant light, we identified critical protein regulators that distinctly couple light-dependent fast reactions with slower biochemical processes in central carbon metabolism. This integrated framework provides scientists with insights to develop testable hypotheses about the roles of gene products and protein regulators in dynamic cellular processes, driving new discoveries in gene regulatory interactions. Overall, our approach is a paradigm shift that offers a robust and adaptable tool for advancing our understanding of cellular responses, with broad applicability for foundational research and bioengineering applications

Materials and Methods

Collection of *S. elongatus* transcriptome datasets

The training datasets were processed from an existing transcriptome database of *S. elongatus*. Raw RNA sequencing (RNA-Seq) data as FASTQ files from the NCBI Sequence Read Archive (SRA, [57]), Gene Expression Omnibus (GEO, [58]) and Joint Genome Institute databases (JGI, [58]) (as of 31 January 2023) were collated into a single training dataset. Overall, the raw RNA-Seq dataset comprised of 386 samples as described in **S1 Table**. Raw sequences were processed using Rsubread [59] and mapped against a set of reference genome sequences: chromosome NC 007604.1, pANL plasmid NC 004073.2, and pANS plasmid NC 004990.1. The resulting mapped RNA-Seq dataset was assessed using FastQC [60] and manually inspected and refined by down selecting only data with a high correlation between biological replicates (>0.9) as well as the associated metadata for the experimental conditions, as described provided in the sourced databases or related peer-reviewed publications [23, 26, 61-66]. In total, the resulting RNA-Seq dataset for PCC 7942 comprised of 330 high-quality RNA-Seq samples (named selongEXPRESS) and is described in **S2 Table**.

Curation of modulated datasets with ICA

We transferred the full gene dataset to a modulated data set where the dimensions of the input gene dataset were reduced using ICA on the iModulonDB [10] web platform. The log-transformed transcripts per million (TPM) gene count samples that passed the QC pipeline were used as input for ICA (**S3 Table**). Then, ICA was performed to calculate the independent M and A significance matrices (**S4 and S5 Tables**), which correspond to the contribution of each gene to the statistical independent source of variation in the modules and the module signal strength for a given condition respectively.

The reduced model consists of a set of “perturbations”, “molecular transcription factors”, and “phenotype module responses”. We explained these terms as follows:

- (a) The perturbations are the light intensities and circadian time encoding values. The 24-hr circadian time encoding features were combined into two vectors (i.e. “Hour Sin” and “Hour Cos”) via the sin-cos transformations of the light intensity incident on the sample. Perturbation encodings are described in **S2 Table**.
- (b) The molecular TFs were identified using the P2TF [67], ENTRAF [68], and DeepTFactor [69] pipelines with a subset of TFs selected based on whether they had a significant circadian phase as determined by Markson *et al.* [44]. We also included an additional set of TFs of interest in response to light perturbations and circadian cycles, that were not previously identified by Markson *et al.* [44].

Their TFs were the master circadian regulators (RpaA & RpaB), the heat shock response proteins responding for changes in light conditions (Rre1 & HrcA), and the master nitrogen regulator (NtcA) [65, 70]. [69] pipelines, with a subset of transcription factors selected based on whether they had a significant circadian phase as determined by Markson *et al.* [44]. Their TFs were the master circadian regulators (RpaA & RpaB), the heat shock response proteins responding to changes in light conditions (Rre1 & HrcA), and the master nitrogen regulator (NtcA) [65, 70].

- (c) The phenotype module responses were captured as the gene differential expression with $|\log_2 \text{fold}| > 1$ when using a subset of the RNA-seq data provided under the Project_tag “Light” from the selongEXPRESS dataset described above. The differential expression for each encoded timepoint between dawn time zero and the time of perturbation was calculated with DESeq2 [71] against high light-intensity dawn conditions (see **S6-S8 Tables**).

Training system-level PIML models with the CellBox package

We utilized the CellBox package to predict the responses of each node under perturbation conditions by generating and solving the ordinary differential equation system in **Eq 1** with the long-time steady-state expression level that offers the predictions.

$$\frac{dg_i(t)}{dt} = \epsilon_i \tanh\left(\sum_{j \neq i} \omega_{ij} g_j(t) + p_i(t)\right) - \alpha_i g_i(t) \quad (1)$$

The CellBox package uses a neural-network architecture to learn the parameters within an interaction-decay response function, which models the expression level of the i -th gene, $g_i \in \mathbb{R}$, under perturbation $p_i \in \mathbb{R}$, where \mathbb{R} is the set of real numbers. The effective interactions between the different genes are modelled through the connectivity matrix $\omega \in \mathbb{R}^{|g| \times |g|}$, while the decay of expressed proteins is modelled through the decay constants $\alpha \in \mathbb{R}^{|g|}$. The proportion that the interactions affect a genes expression is encoded within the scaling constant $\epsilon_i \in \mathbb{R}$, with the sigmoidal hyperbolic tangent envelope function highlighting the significant interactions. The model parameters $\{\epsilon, \omega, \alpha\}$ are learnt through the neural-network architecture to minimize a loss function when compared to expected gene expression values for each perturbation condition p . The values of these parameters are then analyzed to infer gene-gene interactions in the network.

Here, we used the mathematical framework of the CellBox package to infer gene interactions within selected expression data measured with well-characterized perturbations and metadata, such as the incident light levels in the circadian experiment. The light intensity and photon flux/cycle time metadata were encoded into system perturbations, as photons per micromole per second, which allow us to explore the effects of light on the cell system.

The input for CellBox is consisted of normalized TF expression profiles, perturbation encodings, and module expression profiles. The input expression levels were normalized by subtracting the logTPM expression levels of the dawn ($t = 0.5$ h) condition, leading to a set of perturbed conditions from which CellBox predicted expressions. The procedure to transform the data sets of expression profiles into a spreadsheet of input files as well as the steps to train the PIML models using CellBox are provided in the **Sections 3 and 5 of S1 Text**, respectively.

To explore the combination of gene expressions and modules that produce the most effective CellBox models, a range of combinatorial input datasets were generated which concentrated on one specific system or expressing perturbation strength as a log2 fold change in gene/module expression. To train on the datasets of the Gene or Module model, we execute CellBox to sweep through the parameter spaces of up to 1000 combinatorial candidates. The learning loss function was used to determine the best candidate. The validation loss during the machine-learning procedure was defined as the Euclidean distance between the physics-informed response model (**Eq 1**) and the experimental reference data (please see the **S1 Text**). This loss value was used as the prediction accuracy to evaluate the candidates.

The best models returned from the CellBox package were analyzed to determine the inferred interaction networks. The significant gene or module interactions were defined from the output network by using an FDR adjusted t-test, in which edge interactions were tested for a significant difference, with edges with a p-value greater than 0.023 (or 0.015) being retained for the Module (or Gene) model, respectively.

Construction and interpretation of a reduced regulatory network

Taking the best models trained by CellBox, networks were then represented as graphs to facilitate the interpretability of the outcomes for both the Module and Gene models. This network of a reduced regulatory system demonstrates how the pairwise interactions [72] advance the understanding of the causal interactions within the corresponding curated datasets. We used the values within the parameter matrix ω in **Eq 1** that contain the interaction information to capture the influence from the other genes or modules on a given gene. These values can be used to draw an interaction network on a graph where the nodes are the set of genes or modules, and the edges show the interactions. The network interactions for both the Module and Gene models were analyzed to highlight the significant interactions justified by the one-sided

t-test which queries the significance in the learnt interaction strengths when compared to the null hypothesis of no interaction. Please see **Section S4** of **S1 Text** for more details.

Global and redox proteome experiments

Global and redox proteome experiments were performed to understand the regulatory dynamics of carbon fixation in *S. elongatus* PCC 7942 cscB/SPS. This microbe was cultured in a modified BG-11 medium 0.09 g L⁻¹ Yeast Nitrogen Base without amino acids and ammonium sulfate (H26271.36, Thermo Fisher Scientific Inc., USA), 0.264 g L⁻¹ of (NH₄)₂SO₄ (J64180.A1, Thermo Fisher Scientific Inc., USA), 0.174 g L⁻¹ of K₂HPO₄, (60,356, Sigma-Aldrich, USA), and 1 mM of isopropyl-β-d-thiogalactopyranoside (I56000, RPI, USA) at 30°C with a 1% CO₂ supply. The culture was exposed to constant light (~650 μmol m⁻² s⁻¹) for 6 days then diluted with spent culture media to an OD_{750nm} of 0.08 (to enable full and equal light availability in the culture) and cultured under lights for 30 min.

Three biological replicates for each treatment were prepared as follows. The light treatment samples were harvested following the 30 min of light exposure, while the dark treatment cultures were transitioned to the dark (light turned off, culture flasks wrapped in foil) and incubated for an additional 2 hr before collection and sample processing. For each biological replicate, 100 mL of culture was split into two 50 mL aliquots and centrifuged at 4,700 g for 5 minutes at 4°C. The sample supernatant was decanted, and the cell pellets were flash frozen in liquid nitrogen and stored at -80°C. Dark treatment samples were kept in the dark during these processing steps. Next, samples were processed as described previously [37]. Briefly, cell pellets were treated with 10% cold trichloroacetic acid on ice. Then, cells were incubated in 250 mM HEPES (pH 7.5) containing 8 M urea, 10 mM ethylenediaminetetraacetic acid (EDTA), 0.5% sodium dodecyl sulfate (SDS), and 100 mM N-ethylmaleimide (NEM) for 2 h, then lysed by bead beating. The extracted protein was precipitated and washed with cold acetone, then reduced with dithiothreitol. The reduced protein was further processed with a resin-assisted capture (RAC) protocol to selectively enrich proteins with oxidized cysteine residues [73]. The detailed experimental procedure for redox proteome is further described elsewhere [74].

At the same time, an aliquot was taken from each protein sample before resin-assisted capture enrichment to quantify the global protein expression level. Isobaric labeling was used to assist quantification. The enriched samples and global protein samples were analyzed by a nanoAcquity UPLC system (Waters) coupled to a Q-Exactive HF-X Orbitrap mass spectrometer (Thermo Scientific, San Jose, CA) in 120-min liquid chromatography (LC) gradient. A full mass spectroscopy (MS) scan was acquired in the range of m/z = 400 – 1800. MS/MS was performed in a data-dependent mode. The parent ion tolerance was 20 ppm. LC-MS/MS raw data were searched against the *S. elongatus* PCC 7942 UniProt

database (downloaded on March 8, 2022) using MS-GF+ [73, 75]. The detailed experimental procedure is further described elsewhere [73].

Word cloud analysis

The proteomic results were filtered by a spectral-level FDR of less than 1%, based on a target-decoy strategy and MSGFDB_SpecEValue $< 1 \times 10^{-8}$. Data analysis was performed using R. The expression measurements were analyzed for significance. Values with a log2 fold change > 0.1 or < -0.1 with a p-value < 0.05 were considered significant. These genes were cross-referenced with the sets of significant genes returned by the computational analyses to highlight mechanical importance, with results from the computational workflow from this study. Word clouds were formed by comparing the significant changes in gene expression between the PIML models and in the proteome expression data. Please see **Figure 5**.

Acknowledgments

The research described in this paper is part of the Predictive Phenomics Initiative and was conducted under the Laboratory Directed Research and Development Program at Pacific Northwest National Laboratory (PNNL). This work is also partially supported by the NW-BRaVE for Biopreparedness project funded by the U. S. Department of Energy (DOE), Office of Science, Office of Biological and Environmental Research, under FWP 81832. A portion of research was performed using the Tahoma Computing Facility at the Environmental Molecular Sciences Laboratory (EMSL) and using resources available through Research Computing at PNNL. PNNL is a multi-program national laboratory operated by Battelle for the DOE under Contract DE-AC05-76RLO 1830.

Author contributions

M.S.C., S.F., W.Q., T.Z., P.B. designed the research. C.J., Z.J., L.M., S.F., X.L., N.S. performed the research. M.S.C., C.J., Z.J., X.L., S.F. analyzed data. All authors contributed to writing the paper.

References

1. Puszynska, A.M. and E.K. O'Shea, *Switching of metabolic programs in response to light availability is an essential function of the cyanobacterial circadian output pathway*. eLife, 2017. **6**: p. e23210.
2. Treece, T.R., et al., *Synthetic Biology Approaches for Improving Chemical Production in Cyanobacteria*. Frontiers in Bioengineering and Biotechnology, 2022. **10**.

3. Flamholz, A.I., et al., *Revisiting Trade-offs between Rubisco Kinetic Parameters*. Biochemistry, 2019. **58**(31): p. 3365-3376.
4. François, J.M., C. Lachaux, and N. Morin, *Synthetic Biology Applied to Carbon Conservative and Carbon Dioxide Recycling Pathways*. Frontiers in Bioengineering and Biotechnology, 2020. **7**.
5. Misra, B.B., et al., *Integrated omics: tools, advances and future approaches*. Journal of Molecular Endocrinology, 2019. **62**(1): p. R21-R45.
6. Zhang, B. and B. Kuster, *Proteomics Is Not an Island: Multi-omics Integration Is the Key to Understanding Biological Systems*. Mol Cell Proteomics, 2019. **18**(8 suppl 1): p. S1-S4.
7. Lopez, R., et al., *Deep generative modeling for single-cell transcriptomics*. Nature Methods, 2018. **15**(12): p. 1053-+.
8. Xue, Y.F., M.Q. Ding, and X.H. Lu, *Learning to encode cellular responses to systematic perturbations with deep generative models*. Npj Systems Biology and Applications, 2020. **6**(1).
9. Köbis, M.A., A. Bockmayr, and R. Steuer, *Time-Optimal Adaptation in Metabolic Network Models*. Front Mol Biosci, 2022. **9**: p. 866676.
10. Rychel, K., et al., *iModulonDB: a knowledgebase of microbial transcriptional regulation derived from machine learning*. Nucleic Acids Res, 2021. **49**(D1): p. D112-D120.
11. Wu, F.Y., et al., *Single-cell profiling of tumor heterogeneity and the microenvironment in advanced non-small cell lung cancer*. Nature Communications, 2021. **12**(1).
12. Li, C.B., et al., *Single-cell transcriptomics reveals cellular heterogeneity and molecular stratification of cervical cancer*. Communications Biology, 2022. **5**(1).
13. Kamimoto, K., et al., *Dissecting cell identity via network inference and in silico gene perturbation*. Nature, 2023. **614**(7949): p. 742-+.
14. Zhou, H., et al., *Cysteine thiol-based post-translational modification: What do we know about transcription factors?* Trends in Plant Science, 2023. **28**(4): p. 415-428.
15. Lee, I.G. and B.J. Lee, *How Bacterial Redox Sensors Transmit Redox Signals via Structural Changes*. Antioxidants (Basel), 2021. **10**(4).
16. Patel, A., et al., *Proteome allocation is linked to transcriptional regulation through a modularized transcriptome*. Nature Communications, 2024. **15**(1): p. 5234.
17. Fang, X., et al., *Nonequilibrium physics in biology*. Reviews of Modern Physics, 2019. **91**(4): p. 045004.
18. Qian, H., et al., *A framework towards understanding mesoscopic phenomena: Emergent unpredictability, symmetry breaking and dynamics across scales*. Chemical Physics Letters, 2016. **665**: p. 153-161.
19. N.C. Sadler, et al., *Live cell chemical profiling of temporal redox dynamics in a photoautotrophic cyanobacterium*. ACS Chemical Biology, 2014. **9**: p. 291-300.
20. Mejia-Rodrigue, D., et al., *PTM-Psi: A python package to facilitate the computational investigation of post-translational modification on protein structures and their impacts on dynamics and functions*. Protein Science, 2023. **32**: p. e4822.
21. Anderson, P.W., *More Is Different*. Science, 1972. **177**(4047): p. 393-396.
22. Onuchic, J.N. and P.G. Wolynes, *ENERGY LANDSCAPES, GLASS TRANSITIONS, AND CHEMICAL-REACTION DYNAMICS IN BIOMOLECULAR OR SOLVENT ENVIRONMENT*. Journal of Chemical Physics, 1993. **98**(3): p. 2218-2224.
23. Puszyńska, A.M. and E.K. O'Shea, *ppGpp Controls Global Gene Expression in Light and in Darkness in S. elongatus*. Cell Rep, 2017. **21**(11): p. 3155-3165.
24. Diamond, S., et al., *The circadian oscillator in <i>Synechococcus elongatus</i> controls metabolite partitioning during diurnal growth*. Proceedings of the National Academy of Sciences, 2015. **112**(15): p. E1916-E1925.
25. Yasuda, A., D. Inami, and M. Hanaoka, *RpaB, an essential response regulator for high-light stress, is extensively involved in transcriptional regulation under light-intensity upshift conditions in Synechococcus elongatus PCC 7942*. J Gen Appl Microbiol. , 2022. **66**: p. 73-79.
26. Fleming, K.E. and E.K. O'Shea, *An RpaA-Dependent Sigma Factor Cascade Sets the Timing of Circadian Transcriptional Rhythms in Synechococcus elongatus*. Cell Rep, 2018. **25**(11): p. 2937-2945 e3.
27. Reel, P.S., et al., *Using machine learning approaches for multi-omics data analysis: A review*. Biotechnol Adv., 2021. **49**: p. 107739.
28. Umarov, R., Y. Li, and E. Amer, *DeepCellState: An autoencoder-based framework for predicting cell type specific transcriptional states induced by drug treatment*. PLoS Comput Biol., 2021. **17**: p. e1009465.
29. Yuan, B., et al., *CellBox: Interpretable Machine Learning for Perturbation Biology with Application to the Design of Cancer Combination Therapy*. Cell Syst, 2021. **12**(2): p. 128-140 e4.

30. Bunne, C., et al., *Learning single-cell perturbation responses using neural optimal transport*. Nature Methods, 2023. **20**(11): p. 1759-1768.
31. Qiu, X., et al., *Mapping transcriptomic vector fields of single cells*. Cell, 2022. **185**(4): p. 690-711.e45.
32. Karniadakis, G.E., et al., *Physics-informed machine learning*. Nature Reviews Physics, 2021. **3**: p. 422-440.
33. Molinelli, E.J., et al., *Perturbation Biology: Inferring Signaling Networks in Cellular Systems*. Plos Computational Biology, 2013. **9**(12).
34. Sastry, A.V., et al., *The Escherichia coli transcriptome mostly consists of independently regulated modules*. Nature Communications, 2019. **10**(1): p. 5536.
35. Choe, D., et al., *Advancing the scale of synthetic biology via cross-species transfer of cellular functions enabled by iModulon engraftment*. Nature Communications, 2024. **15**(1): p. 2356.
36. Markson, J.S., et al., *Circadian control of global gene expression by the cyanobacterial master regulator RpaA*. Cell, 2013. **155**: p. 1396-1408.
37. Guo, J., et al., *Proteome-wide light/dark modulation of thiol oxidation in cyanobacteria revealed by quantitative site-specific redox proteomics*. Mol Cell Proteomics, 2014. **13**(12): p. 3270-85.
38. Min, H. and S.S. Golden, *A new circadian class 2 gene, opcA, whose product is important for reductant production at night in Synechococcus elongatus PCC 7942*. J Bacteriol, 2000. **182**(21): p. 6214-21.
39. Foyer, C.H., *Reactive oxygen species, oxidative signaling and the regulation of photosynthesis*. Environ Exp Bot, 2018. **154**: p. 134-142.
40. Kremer, M., et al., *Bacteria employ lysine acetylation of transcriptional regulators to adapt gene expression to cellular metabolism*. Nature Communications, 2024. **15**(1): p. 1674.
41. Vijayan, V., R. Zuzow, and E.K. O'Shea, *Oscillations in supercoiling drive circadian gene expression in cyanobacteria*. Proc Natl Acad Sci U S A, 2009. **106**(52): p. 22564-8.
42. Nishiwaki, T., et al., *Role of KaiC phosphorylation in the circadian clock system of Synechococcus elongatus PCC 7942*. Proc Natl Acad Sci U S A, 2004. **101**(38): p. 13927-32.
43. Hanaoka, M., et al., *RpaB, another response regulator operating circadian clock-dependent transcriptional regulation in Synechococcus elongatus PCC 7942*. J Biol Chem, 2012. **287**(31): p. 26321-7.
44. Markson, J.S., et al., *Circadian Control of Global Gene Expression by the Cyanobacterial Master Regulator RpaA*. Cell, 2013. **155**(6): p. 1396-1408.
45. Welkie, D.G., et al., *A Hard Day's Night: Cyanobacteria in Diel Cycles*. Trends Microbiol, 2019. **27**(3): p. 231-242.
46. Ohbayashi, R., et al., *DNA replication depends on photosynthetic electron transport in cyanobacteria*. FEMS Microbiol Lett, 2013. **344**(2): p. 138-44.
47. Watanabe, S., et al., *Light-dependent and asynchronous replication of cyanobacterial multi-copy chromosomes*. Mol Microbiol, 2012. **83**(4): p. 856-65.
48. Diamond, S., et al., *Redox crisis underlies conditional light-dark lethality in cyanobacterial mutants that lack the circadian regulator, RpaA*. Proc Natl Acad Sci U S A, 2017. **114**(4): p. E580-E589.
49. Uhlmann, F., *SMC complexes: from DNA to chromosomes*. Nature Reviews Molecular Cell Biology, 2016. **17**(7): p. 399-412.
50. Schmidt, A., *A thioredoxin-activated fructose-1,6-bisphosphatase from the cyanobacterium Synechococcus 6301*. Planta, 1981. **152**(2): p. 101-4.
51. Mallen-Ponce, M.J., M.J. Huertas, and F.J. Florencio, *Exploring the Diversity of the Thioredoxin Systems in Cyanobacteria*. Antioxidants (Basel), 2022. **11**(4).
52. Hagen, K.D. and J.C. Meeks, *The unique cyanobacterial protein OpcA is an allosteric effector of glucose-6-phosphate dehydrogenase in Nostoc punctiforme ATCC 29133*. J Biol Chem, 2001. **276**(15): p. 11477-86.
53. Westermarck, S. and R. Steuer, *Toward multiscale models of cyanobacterial growth: a modular approach*. Frontiers in Bioengineering and Biotechnology, 2016. **4**: p. 95.
54. Cretel, E., et al., *How Cells feel their environment: a focus on early dynamic events*. Cell Mol Bioeng, 2008. **1**(1): p. 5-14.
55. Farrokh, P., et al., *Cyanobacteria as an eco-friendly resource for biofuel production: A critical review*. Biotechnol Prog, 2019. **35**(5): p. e2835.
56. Xing, J., *Reconstructing data-driven governing equations for cell phenotypic transitions: integration of data science and systems biology*. Physical Biology, 2022. **19**: p. 061001.
57. Sayers, E.W., et al., *Database resources of the national center for biotechnology information*. Nucleic Acids Res, 2022. **50**(D1): p. D20-D26.

58. Grigoriev, I.V., et al., *The genome portal of the Department of Energy Joint Genome Institute*. Nucleic Acids Res, 2012. **40**(Database issue): p. D26-32.
59. Liao, Y., G.K. Smyth, and W. Shi, *The R package Rsubread is easier, faster, cheaper and better for alignment and quantification of RNA sequencing reads*. Nucleic Acids Res, 2019. **47**(8): p. e47.
60. Andrews, S., *FastQC: A Quality Control Tool for High Throughput Sequence Data*. 2010: <https://www.bioinformatics.babraham.ac.uk/projects/fastqc/>.
61. Ruffing, A.M., *RNA-Seq analysis and targeted mutagenesis for improved free fatty acid production in an engineered cyanobacterium*. Biotechnol Biofuels, 2013. **6**(1): p. 113.
62. Piechura, J.R., K. Amarnath, and E.K. O'Shea, *Natural changes in light interact with circadian regulation at promoters to control gene expression in cyanobacteria*. Elife, 2017. **6**.
63. Billis, K., et al., *Comparative transcriptomics between Synechococcus PCC 7942 and Synechocystis PCC 6803 provide insights into mechanisms of stress acclimation*. PLoS One, 2014. **9**(10): p. e109738.
64. Vijayan, V., I.H. Jain, and E.K. O'Shea, *A high resolution map of a cyanobacterial transcriptome*. Genome Biol, 2011. **12**(5): p. R47.
65. Choi, S.Y., et al., *Transcriptome landscape of Synechococcus elongatus PCC 7942 for nitrogen starvation responses using RNA-seq*. Sci Rep, 2016. **6**: p. 30584.
66. Simkovsky, R., et al., *Transcriptomic and Phenomic Investigations Reveal Elements in Biofilm Repression and Formation in the Cyanobacterium Synechococcus elongatus PCC 7942*. Front Microbiol, 2022. **13**: p. 899150.
67. Ortet, P., et al., *P2TF: a comprehensive resource for analysis of prokaryotic transcription factors*. BMC Genomics, 2012. **13**.
68. Ledesma, L., R. Hernandez-Guerrero, and E. Perez-Rueda, *Prediction of DNA-Binding Transcription Factors in Bacteria and Archaea Genomes*. Methods Mol Biol, 2022. **2516**: p. 103-112.
69. Kim, G.B., et al., *DeepTFactor: A deep learning-based tool for the prediction of transcription factors*. Proc Natl Acad Sci U S A, 2021. **118**(2).
70. Fadi Aldehni, M., et al., *Signal transduction protein P(II) is required for NtcA-regulated gene expression during nitrogen deprivation in the cyanobacterium Synechococcus elongatus strain PCC 7942*. J Bacteriol, 2003. **185**(8): p. 2582-91.
71. Love, M.I., W. Huber, and S. Anders, *Moderated estimation of fold change and dispersion for RNA-seq data with DESeq2*. Genome Biol, 2014. **15**(12): p. 550.
72. Sarmah, D., et al., *Network inference from perturbation time course data*. NPJ Syst Biol Appl, 2022. **8**(1): p. 42.
73. Guo, J., et al., *Resin-assisted enrichment of thiols as a general strategy for proteomic profiling of cysteine-based reversible modifications*. Nat Protoc, 2014. **9**(1): p. 64-75.
74. Gaffrey, M.J., et al., *Resin-Assisted Capture Coupled with Isobaric Tandem Mass Tag Labeling for Multiplexed Quantification of Protein Thiol Oxidation*. J Vis Exp, 2021(172).
75. Kim, S. and P.A. Pevzner, *MS-GF+ makes progress towards a universal database search tool for proteomics*. Nat Commun, 2014. **5**: p. 5277.

Supporting information

S1 Text. Supplementary Text.

S1 Spreadsheet. S1-S8 Tables, listed below:

S1 Table. Overview of the raw RNA sequencing data .

S2 Table. High-quality RNA-seq dataset, "selongEXPRESS", that passed the quality control.

S3 Table. Transformed gene counts for the selongEXPRESS dataset that passed the quality control.

S4 Table. Calculated independent A significance matrix.

S5 Table. Calculated independent M significance matrix.

S6 Table. Gene expression log2 fold changes calculated using DESeq2.

S7 Table. Standard error values for the log2 fold changes calculated using DESeq2.

S8 Table. Adjusted p-values for the log2 fold changes calculated using DESeq2.